# Excessive Delivery of Nanostructured Matter to Submersed Cells Caused by Rapid Gravitational Settling

**Klaus Wittmaack***

Helmholtz Zentrum München, Institute of Radiation Protection, 85758 Neuherberg, Germany

**ABSTRACT** With very few exceptions, previous nanotoxicity studies implicitly involved the assumption that the techniques developed for risk assessment of hazardous chemical substances can be applied in unchanged form to explore cell response in NP laden media. This misleading approach has the consequence that the actual dose of exposure is ill defined or, more often, completely unknown. Here the effect of gravitational settling on the dose of exposure was explored for commercially available engineered nanostructured matter (nanopowder). Micrometer sized aggregates abundantly present in all nanopowders were fractured as much as possible by probe-type sonication in water or cell culture media. The morphology of cracked aggregates was studied by scanning electron microscopy. Size distributions were determined by dynamic light scattering (DLS). Possible pitfalls encountered in using DLS were documented. Absorbance measurements and optical microscopy served to monitor the rate of gravitational settling on time sales ranging from minutes up to several days. The sonicated particles settled rapidly in all liquid media. At the well bottom, they exhibited intense lateral (two-dimensional) Brownian-like motion, which allowed them to travel large distances. Taken together, the probability for particle–cell contact may be enhanced by a factor of more than 1000 compared to the commonly advocated picture. The very high levels of exposure can give rise to overload effects which are often misinterpreted as evidence of cytotoxicity. To identify the true toxic potential of NPs, future studies must account for these phenomena. It is also argued that stable dispersions of NPs are not required in nanotoxicity studies.

**KEYWORDS:** nanoparticles · nanotoxicity · gravitational settling · *in vitro* studies · Brownian-like motion

Nanotoxicology, that is, research aimed at exploring health risks due to exposure to nanoparticles (NPs) or nanostructured matter, is a rather young scientific discipline that became fully established only about 5 to 6 years ago. Nevertheless, the state of the art has already been reviewed from a large variety of perspectives. The conclusions of the reviews, of which only a small fraction can be cited here,[1−16] were typically of the form:[8] "At the current stage in nanoparticle safety research, it would be premature to conclude, ..., that nanoparticles are inherently dangerous." This cautious wording implies that research performed so far has not led to a reasonable understanding of NP-related risks. The unsatisfactory state of the art raises the question whether or not the previous work always involved meaningful concepts and adequate methodology. Particular attention must be devoted to *in vitro* studies because they constitute the vast majority of investigations in the field. The most unsatisfactory aspect of the previous *in vitro* studies is the implicit assumption that the issue of NP toxicity can be resolved by applying techniques developed for risk assessment of hazardous chemical substances, dissolved or dispersed in molecular form.[16−18] Insoluble NPs suspended in liquid media, however, behave quite differently: they are subject to gravitational forces; they interact with each other as well as with additives contained in the medium; they can form agglomerates; and they may exhibit unidirectional diffusion if concentration gradients are established by the action of the cells.[18,19]

In the vast majority of previous *in vitro* nanotoxicity studies, the NPs were assumed to be uniformly distributed in the suspension,[20,21] as sketched in Figure 1A. The situation changes completely if NPs travel fairly rapidly to the bottom of the well (see Figure 1B). As a result, their concentration in the vicinity of the cells will be much larger than in the situation of Figure 1A. Let $c_M$ be the mass concentration of insoluble matter dispersed in a cell culture medium of height $h$. If all matter would settle at the bottom of the well in a uniform layer, the areal mass density (mass per unit area) $\Theta_M^0$ will be

$$\Theta_M^0 = c_M h \qquad (1)$$

Note that $\Theta_M^0$ is directly proportional to the height $h$. This important aspect of *in vitro* NP dosimetry has long been ignored. Evidence in support of this line of thinking has been presented only very recently.[18] Converted to a compact layer of thickness $w^0$, eq 1 reads

$$w^0 = \frac{\Theta_M^0}{\rho} = \frac{c_M h}{\rho} \qquad (2)$$

* Address correspondence to wittmaack@helmholtz-muenchen.de.

Received for review January 11, 2011 and accepted March 29, 2011.

**Published online March 29, 2011**
10.1021/nn200112u

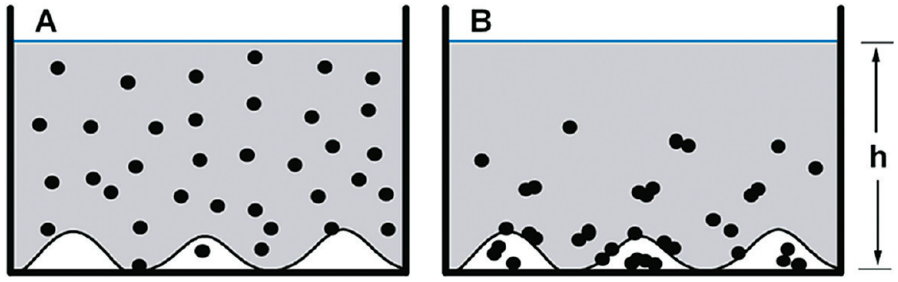


**Figure 1. Schematic illustrations of the conceivable interaction of insoluble particles with submersed cells grown at the bottom of a well, filled with an appropriate medium of height *h*. (A) Previously employed picture, (B) more appropriate concept discussed in this study. The number of particles in (A) and (B) is the same.**

where $\rho$ is the mass density of the NP material. For a quantitative estimate of $\Theta_M^0$ and $w^0$, consider an *in vitro* experiment with a moderate mass concentration of 50 $\mu$g/mL ($\cong$50 $\mu$g/cm$^3$) and $h$ = 0.5 cm. Then $\Theta_M^0$ = 25 $\mu$g/cm$^2$. For NPs composed of carbon or $TiO_2$, that is, with $\rho$ = 2.2 and 3.9 g/cm$^3$, respectively, we have $w^0$ = 114 and 64 nm, respectively. If this unexpectedly large amount of material were delivered to cells, one could hardly be surprised if the normal vital functions would be affected very strongly.

In reality, one has to assume that not the total mass density $\Theta_M^0$ but only a smaller amount $\Theta_M$ will have arrived at the bottom of the well where the cells are residing,

$$\Theta_M(h, v, t) = \eta(h, v, t)\Theta_M^0 \quad (3)$$

The fraction $\eta(h,v,t)$ will depend on the height $h$, the transport velocity $v$ of the NPs (primary particles, aggregates, or agglomerates), and the time $t$ of exposure. The key point is that, without knowing $\eta(h,v,t)$, the response of cells to NP exposure cannot be interpreted in a quantitative manner because the actual dose is not known. Only very few groups have reported relevant data. Convincing evidence for efficient NP transport to submersed human lung fibroblast cells was reported for flame synthesized ceria particles in the size range of 25 to 500 nm.[19] NP uptake by the cells proceeded at a roughly constant rate, for exposures up to 4 h. The measured data were interpreted in terms of transport by diffusion of the (agglomerated) small NPs and by gravitational settling of particles in the large size fraction. Aspects of NP toxicity, however, were not explored.

The missing correlation was identified very recently in a reanalysis[18] of published data containing information on the uptake of ~30 nm silica particles as well as on the associated cytotoxicity induced in three different cell lines.[22] The most important results of the data evaluation were as follows:[18] (i) NP uptake depended not only on the mass concentration but also on the height of the medium. (ii) The results could only be explained if, in addition to diffusion, gravitational settling of agglomerated NPs contributed significantly to the transport of matter to the cells. (iii) Loss of viability became observable only if cells were exposed to the equivalent of one to five layers of NPs; the dose required for complete cell death ranged between 4 and about 20 layers of NPs.

In view of these findings, it appeared highly desirable to explore NP transport to cells for commercially available engineered NPs,[23] also referred to as nanopowders. The toxic potential of this kind of material has received considerable interest recently.[20,24] One should note, however, that most of the primary NPs contained in nanopowders are tightly bound to each other in much larger aggregates.[25,26] Typically 99% of the mass of typical nanopowders was found in the size range above 1 $\mu$m.[26] Whereas the size distributions of sonicated matter dispersed in different media were studied in great detail by dynamic light scattering (DLS),[20,24] transport to the bottom of cell culture vials has not yet received much attention.

The purpose of this study was to determine the time and height dependent fraction $\eta(t,v,h)$ of settled NP matter. It turned out to be necessary to pay much attention to a characterization of the sonicated matter by scanning electron microscopy (SEM), DLS, and absorbance measurements. Finally, the aim was to enter into an exploratory investigation of the interaction of settled NPs with cells under conditions frequently used in nanotoxicity studies.

## RESULTS

**Aggregate Size, As Delivered and after Sonication.** SEM images of nanopowders in different stages of sample preparation are presented in Figure 2. The nanopowders were first dissolved in the specified liquids; 1 $\mu$L aliquots were subsequently deposited on polished silicon substrates and allowed to dry in ambient air. Two examples of aggregates are shown in Figure 2A,B for $TiO_2$(80) and $Fe_2O_3$(60), respectively (the numbers in parentheses denote the mean primary particle size in nanometers). Prior to deposition, the powders were gently mixed in high-purity water. In both cases, the aggregates are seen to be composed of primary particles, tightly attached to each other, more so for $Fe_2O_3$ than for the $TiO_2$. The other similarity is that the primary particles exhibit a significant spread in size, with a most probable size commensurate with the size

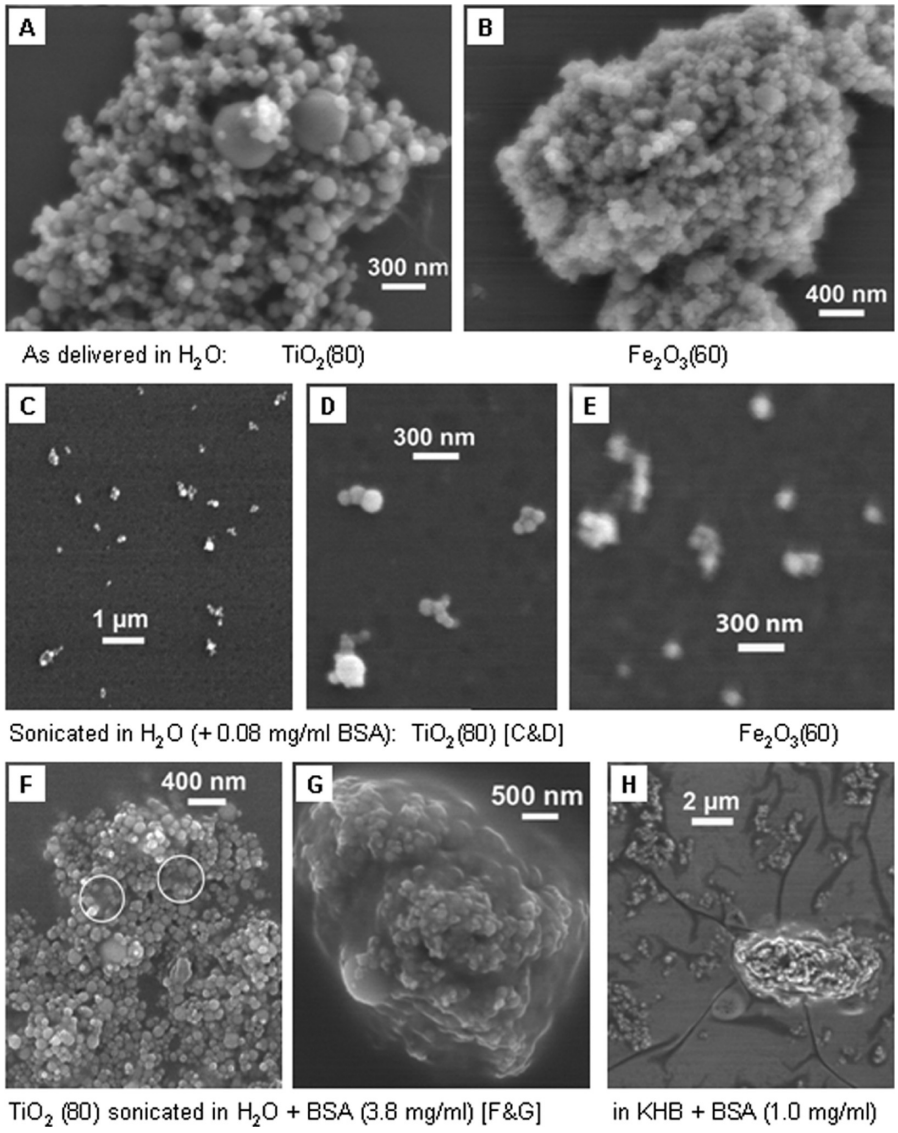


**Figure 2. Scanning electron images of nanopowders initially suspended in the specified media and subsequently dried from 1 $\mu$L droplets deposited on polished silicon substrates.**

numbers quoted by the manufacturer (more correctly manufacturers should refer to the material not as being composed of NPs but rather as being nanostructured). The $TiO_2$(80) powder differed from other oxide powders in that most of the dried deposits formed extended, fairly thin layers, with a thickness equivalent to only a few times the primary particle size. By contrast, the other analyzed samples of dried (or air borne) nanopowders contained bulky aggregates like the one shown in Figure 2B.

The difference between (nontransparent) nanopowders in terms of their content of free or loosely bound primary particles becomes evident by examining the opaqueness of water poured on a sample in a test glass. Likewise, the ease with which aggregates can be broken into smaller pieces shows up *in situ* as progressive opaqueness, increasing with increasing time of sonication. $TiO_2$(80) turned out to particularly easy to break up by sonication, one of the reasons for the frequent use of the material in this study. However, complete break up of $TiO_2$(80) and the other nanopowders could not be achieved. Even at the maximum power possible with a probe-type sonicator (*i.e.*, up to the point beyond which significant erosion of the tip occurs), the ultimate effect of imparting ultrasound energy on aggregates was to detach weakly bound NPs and small nanoaggregates from larger objects (usually the sonicator was operated well below the critical power so that flakes due to tip erosion were not observed). Examples of unbreakable "nanoaggregates", observed after sonication, are depicted in Figure 2C–E. Apparently, the primary particles contained in a nanoaggregate are tightly bound together by sintering during the high-temperature production process so that the forces that can be imparted by sonication are not sufficient to fracture the nanoaggregate at the neck between two primary particles.

The mean particle sizes estimated from the SEM images are in good agreement with the size spectra measured by DLS, as shown by the spectra denoted by solid lines in Figure 3A,B, featuring most probable hydrodynamic diameters of 215 and 210 nm for $TiO_2$-(80) and $Fe_2O_3$(60), respectively. It is worth noting that with nanopowders other than $TiO_2$(80) large nonfractured aggregates (>3 $\mu$m) were frequently observed by SEM, even after prolonged high-power sonication.

To reduce the surface tension of pure water, a small amount of bovine serum albumin (BSA, 0.08 mg/mL) was added to the aqueous suspension prior to drying the samples of Figure 2C−E. This approach served to minimize agglomeration of primary particles during drying. For a 1 $\mu$L droplet covering a circular area with a diameter of typically 1.5 mm after drying, the quoted BSA concentration converts to a layer of 30 nm (assuming uniform thickness and a BSA mass density of 1.5 g/cm$^3$). BSA sticking to NPs and nanoaggregates may enlarge the apparent size and degrade resolution in SEM analysis. This appears to have been the case with the $Fe_2O_3$(60) objects in Figure 2E. By contrast, little or no BSA seems to have attached to the $TiO_2$(80) nanoaggregates seen in Figure 2D.

The importance of SEM imaging of particles in aqueous solutions cannot be underestimated: one gets to know to what extent aggregates can be fractured by sonication. The ultimate goal, of course, would be imaging of nanoaggregates in cell culture media. Unfortunately, this is not possible without very severe artifacts. As documented in Figure 2F,G, with BSA added to an aqueous suspension at a concentration of 3.8 mg/mL (well below the standard 10 mg/mL in cell culture media), the suspended nanoaggregates form various types of agglomerates upon drying. Only a few of the agglomerates are found at the surface of the dried BSA layer which, in the images of Figure 2F,G are estimated to be 1.4 $\mu$m thick. The situation becomes even more complex when nanoaggregates in a dried buffer solution are examined (see Figure 2H) (Krebs-Henseleit buffer, KHB, with 1 mg/mL BSA). The conclusion is that useful information on the agglomeration state of the nanoaggregates in cell culture media cannot be derived by SEM imaging of dried solutions.

**Agglomeration in Cell Culture Media.** The response of nanopowders to sonication in water and cell culture media has been investigated in detail before.[20,24] The results obtained in this study were generally in accordance with the previous work. For example, the mean sizes $\langle x \rangle$ observed by DLS after sonication were always smallest in water. Table 1 shows a compilation of results for two different sonication powers. The effect of increasing the power was moderate, sometimes negligible. The differences in response to sonication reflect the fact that the amount of primary particles and nanoaggregates one may detach from large aggregates differs strongly between nanopowders. Note also that there is no systematic correlation between $\langle x \rangle$ and the primary particle size. Last, but not least, it is worth noting that, owing to the small amount of mass used here in individual experiments (typically between 0.1 and 0.5 mg), one can also expect significant fluctuations in the distribution of aggregates in the raw sample materials. Differences in $\langle x \rangle$ by up to 20% were observed between different experiments under nominally the same conditions. This finding raises the question whether it makes sense to quote measured $\langle x \rangle$ values with three significant digits.[20,24] Two significant digits are more representative of reality.

Sonication in buffer solution or the addition of buffer to a sonicated suspension usually gave rise to pronounced or very pronounced agglomeration, as shown in Figure 3A,B for sonicated $TiO_2$(80) and $Fe_2O_3$-(60). The extent of agglomeration could be reduced significantly by adding BSA or fetal calf serum (FCS) (see Figure 3A). Rather important was the finding that there are very little, if any, differences in the extent of agglomeration for different media, as shown in Figure 3B for $Fe_2O_3$(60) in HAM's nutrient mixture, HAM's F12, and Dulbecco's modified eagle medium (DMEM). In an additional test, $TiO_2$(80) was first sonicated in high-purity water at a concentration of 150 $\mu$g/mL. Then 0.9 mL of KHB + BSA, DMEM + FCS, or RPMI 1640 + FCS was added to 0.1 mL aliquots of the aqueous suspension. The size spectra of all three samples were found to be the same within experimental uncertainty (most probable hydrodynamic diameter 750 ± 30 nm). It is worth mentioning that, in contrast to the most probable size, the width of the distributions can vary significantly in a series of 30 s DLS measurements on the same sample. This observation implies that the size distribution in the analyzed volume can fluctuate significantly.

Another aspect of concern in previous work was the stability of NP solutions during sample storage after preparation, for sonicated nanopowders[20] and NP suspensions synthesized in solution.[22] The aim was to show that the mean diameter of the NPs remained constant. The size distributions observed in this work for nanoaggregates in cell culture media with serum also remained essentially unchanged for periods up to 3 days (see Figure 3B,C). This type of stability, however, does not imply that the number concentration of the suspended particles in the analyzed volume also remained constant. The problem is that a DLS measurement yields only a normalized size distribution, and particle concentrations in absolute terms cannot be derived. In other words, the stability of size distributions does not provide evidence for the absence of gravitational settling or diffusion.[18]

Some rather crude information concerning possible changes in concentration could be derived from the DLS signal due to the large molecules of the serum which, however, feature only a very small scattering

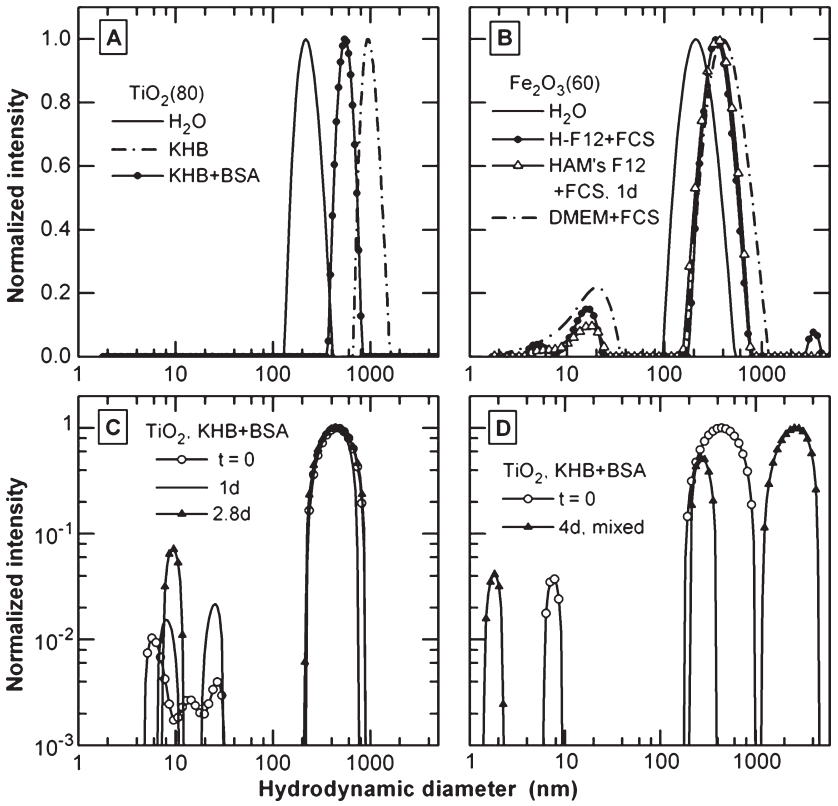


**Figure 3. DLS spectra of sonicated nanopowders measured in a variety of media and at different times of storage after sonication. The height of the analyzed liquid in the DLS cuvette was usually 18 mm. The mass concentrations ranged between 20 and 30 $\mu$g/mL. BSA concentrations: (A) 0.5 mg/mL, (C) 5 mg/mL, and (D) 7 mg/mL. In (B), H-F12 denotes HAM's F12; FCS concentration 10%. The spectrum labeled by solid triangles in (D) was measured following gentle agitation of the suspension after 4 days of sample storage.**

**TABLE 1. Mean Size $\langle x \rangle$ of Nanopowders Dispersed in Water after Probe-Type Sonication at Two Different Ultrasound Powers, 30 and 70% of the Maximum (Labeled "Moderate" and "High", Respectively). Duration typically 1 min. 'Fil' denotes $\langle x \rangle$ after having passed the sonicated solution through a filter with a pore size of 0.22 $\mu$m**

| nanopowder | $\langle x \rangle$ (nm) moderate power | $\langle x \rangle$ (nm) high power |
|---|---|---|
| $TiO_2$(20) | | 190 (±40%) |
| | | Fil: 75 (±30%) |
| $TiO_2$(80) | 190 (±40%) | 120 (±30%) |
| | | Fil: 93 (±25%) |
| $TiO_2$(200) | | 250 (±20%) |
| $Fe_2O_3$(60) | 115 (±40%) | 105 (±50%) |
| $SiO_2$(80) | | 170 (±40%) |
| $Fe_3O_4$(25) | | 220 (±40%) |
| Co(30) | 1100 (±20%) | 1050 (±40%) |
| $CeO_2$(100) | 620 (±25%) | 400 (±40%) |
| Aerosil | 85 (±20%) | 80 (±30%) |
| Printex 90 | 80 (±40%) | 80 (±40%) |
| carbon SWNT | 300 (±40%) | |
| | Fil: 80 (±40%) | |

cross section. In Figure 3C, the BSA signal around 10 nm is somewhat noisy but increases with increasing time of sample storage. If one assumes that the concentration of the serum remains unchanged, at least on the scale of a few days, the increasing BSA signal means that the $TiO_2$ nanoaggregate concentration, arbitrarily normalized to unit peak intensity by the software, actually decreased significantly during the almost 3 days of sample storage. Similar information could be derived by taking note of the laser power which the DLS instrument selects for optimum performance in the respective run. The chosen power is higher the lower the particle concentration. In the measurements of Figure 3C, the optimum power at time 2.8 days was a factor of 3−3.5 higher than for the fresh sample, indicating a loss in concentration during the storage period by roughly the same factor.

**Time-Dependent Decrease in Absorbance as a Means of Quantifying Gravitational Settling.** More quantitatively reliable information on changes in particle concentration, that is, on settling, was derived by measuring the absorbance in parallel with the DLS analysis. Notably, in the case of $TiO_2$, it was found that such measurements must be carried out with great care because the distribution of particles can be distorted by exposure to the beam of light (see below). In order to avoid distortions as much as possible, it is advisible to minimize the time of the measurement. Another problem of somewhat erratic nature was the deposition of particles at the walls of the cuvette. This gave rise to an additional absorbance superimposed on the signal

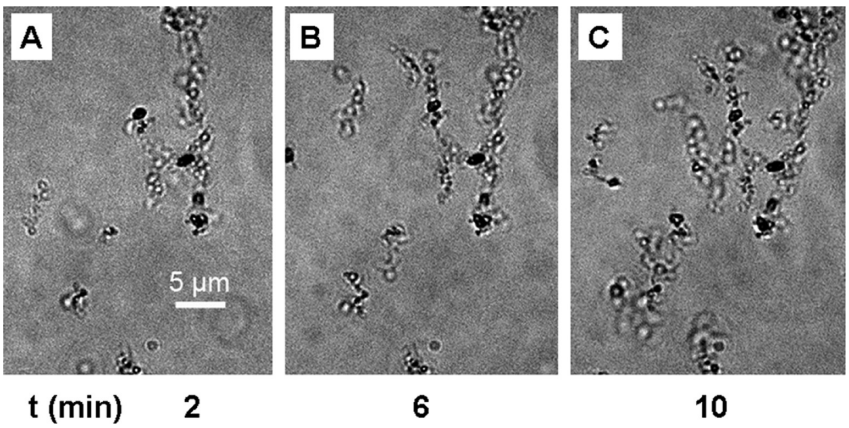


**Figure 4. Time dependence of the settling of $Fe_2O_3$ nanoaggregates suspended in KHB medium and subsequently deposited as a 20 $\mu$L droplet on a coverslip. The images were taken by A. Stampfl.**

due to the medium. The added wall contribution was determined at the end of a measurement after having removed the solution. With these complications in mind, the absorbance after 2.8 days of sample storage was found to be reduced to 15−20%. The conclusion is clear: even though DLS measurements might indicate the stability of size distributions, gravitational settling may cause a severe loss of nanoaggregates from cell culture media with heights as large as 10−20 mm (see Methods).

By far, the largest settling velocity was observed with sonicated nanopowders of cobalt. Settling in water in a DLS cuvette (height 20 mm) was largely complete after only 80 min (residual absorbance <10%). Already after 30 min, the settled matter had caused a blackening of the well bottom that was visible to the naked eye. Remarkably, very significant agglomeration took place in the course of the experiment: the mean size by DLS increased from 830 nm (±40%), 4 min after the end of sonication (2 min at 35% of maximum power), to 1500 nm (±30%) after 60 min. On the basis of Stokes law, or a modification thereof which accounts for agglomeration,[19] the settling velocity $v$ is proportional to the cross section ("area") of the agglomerate and difference $(\rho - \rho_m)$ in the mass densities of NP matter $(\rho)$ and the medium $(\rho_m)$. Owing to the fact that cobalt features a rather high mass density ($\rho_{Co}$ = 8.9 g/cm$^3$), the observed high settling velocity is not really surprising. This reasoning also implies that, for aggregates of the same size and morphology, the settling velocity for carbon ($\rho_C$ = 2.2 g/cm$^3$) should be a factor 7.9/1.2 = 6.6 lower than for cobalt (assuming $\rho_m$ = 1 g/cm$^3$).

**Agglomeration State of Settled Matter.** Attention has also been devoted to the status of the settled matter. For this purpose, a sonicated suspension of $TiO_2$(80) in KHB (plus 7 mg/mL BSA) was allowed to settle for 4 days. Then the settled deposit was redispersed by gently turning the test glass with the stock solution repeatedly upside down. The DLS spectrum of the redispersed matter exhibited two prominent peaks, one centered at 260 nm, the other at 2.7 $\mu$m, as shown in Figure 3D (solid triangles). This observation suggests that significant additional agglomeration took place within the settled matter, giving rise to the 2.7 $\mu$m peak. However, some fraction of the sonicated matter seems to escape agglomeration, retaining its character in the form of individual nanoaggregates (peak at 260 nm). Note also that in this particular measurement the BSA peak is located at the "wrong" position, an artifact presumably due to the presence of the prominent 2.7 $\mu$m peak. In additional runs, the peak was found at other positions or was even absent. Evidently, one has to conclude that the ability of DLS to properly determine the spectrum of multicomponent suspensions is limited.

**Early Stages of Particle Settling and Agglomeration.** An example of the short-term arrival of particles at the bottom of a suspension is presented in Figure 4. $Fe_2O_3$ powder was suspended in KHB, to which 10% (10 mg/mL) BSA was added. After sonication for 2 min at the upper limit of supersonic power, a 20 $\mu$L droplet was deposited on a coverslip and immediately transferred to an inverted microscope. The three images in Figure 4 relate to three different times after sample deposition, as specified below each panel. Inspection of the images shows that during an 8 min period the number density of particles at the bottom of the suspension has roughly doubled. This observation indicates rapid settling. Note also that the particles arrange in the form of agglomerates, preferentially chain-type.

**Rapid Pile-up of Settled Particles at the Bottom of Wells.** Turning to the results obtained by microscopic observation of particle arrival at the bottom of cell culture wells, the time dependence of settling of sonicated $TiO_2$(80) in KHB is documented in Figure 5 for two different heights of the medium. A comparison of Figure 5B,C shows essentially the same coverage: this finding leads to the conclusion that settling in a 3.1 mm high medium (corresponding to 100 $\mu$L of medium) was complete after only about 5 h (or even less). When the height of the medium was increased by a factor of

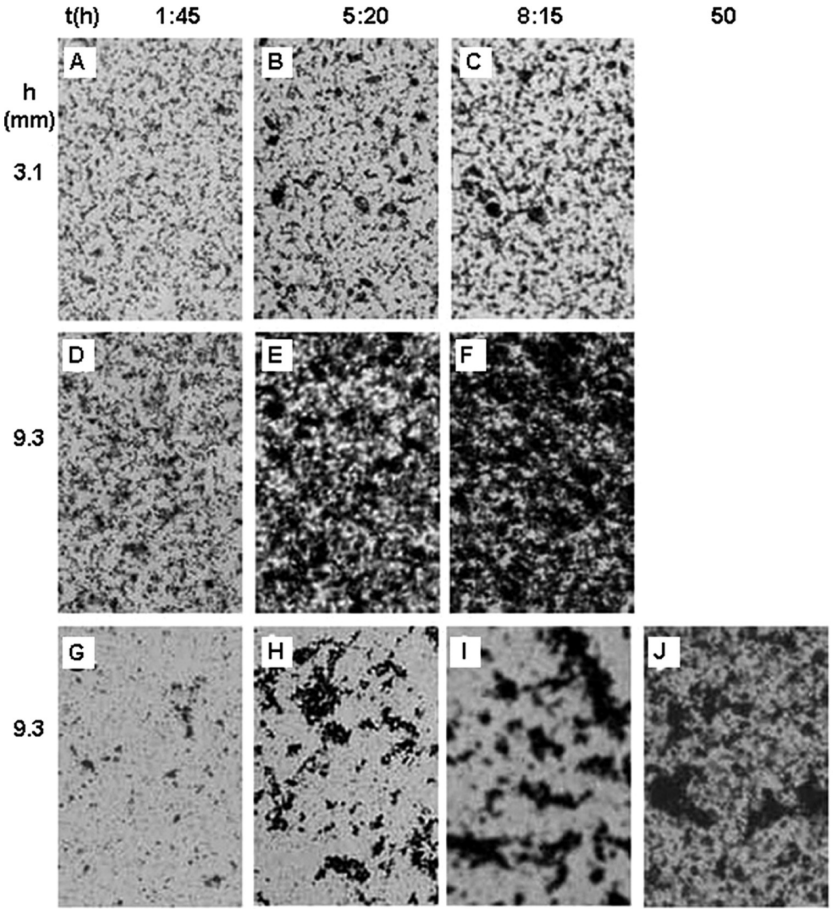


**Figure 5. Time dependence of the settling of $TiO_2$(80) particles (27 $\mu$g/mL) at the bottom of cell culture wells following sonication in KHB medium (96-well plate). The clock was started after having deposited the suspensions in the wells. At the quoted heights, *h*, of the media, the mass concentration converts to maximum achievable areal densities of (A–C) 8.4 $\mu$g/cm$^2$ and (D–J) 25.2 $\mu$g/cm$^2$ (corresponding thicknesses 21.5 and 64.5 nm). Each image is 200 $\mu$m wide. The mean size of the agglomerated nanoaggregates was 980 nm, by DLS. (G–J) Images relate to the same medium as in panels A–F, but with BSA added at 7 mg/mL after sonication (mean agglomerate size 440 nm).**

3, the volume of the settled material increased significantly, as a comparison of the top and center row of images in Figure 5 shows. An important observation in all settling studies was that nanoaggregates come to rest at the bottom of the wells not as a uniform layer but rather in the form of extended fractal deposits. Prior to attaching to larger agglomerates (formed at the early stage of settling; see Figure 4), all particles executed intense Brownian-like motion near the bottom of the well (see below).

In a simple model appropriate for particles of uniform size and identical mean sedimentation velocity, the process of gravitational settling may be considered equivalent to the collection of matter taking place when a suspension is driven through a filter by the action of a piston. If two solutions of different volume contained in cylinders of the same diameter are propelled at the same traverse speed, the amount of filtered particles will be the same until the low volume suspension is exhausted. Using this model, the coverage in Figure 5A,D should be the same. This is evidently not the case. The distinctly higher particle density in Figure 5D is most likely due to the fact that the assumption of a uniform size and settling velocity is not valid. In reality, the suspended particles feature a broad size distribution, as shown in Figure 3. This means that already at comparatively short times, like 1:45 h, the largest agglomerates have apparently been able to travel (significantly) more than 3.1 mm. The large agglomerates present at a height >3.1 mm are considered to be responsible for the difference in coverage in Figure 5A,D. In more dedicated work, this effect may be used to assess the settling velocity of large agglomerates or to deposit them preferentially on cells.

The prediction of eq 2 (*i.e.*, $w^0 \propto h$) was confirmed by a comparison of the mean darkness of Figure 5C,F, which reflect the case of completely settled matter. For a quantitative evaluation, the number density of extended black features with sizes >10 $\mu$m was counted. The ratio for the media with $h$ = 9.3 and 3.1 mm was 3 $\pm$ 0.4, somewhat dependent on the section of the total image analyzed (the panels of Figure 5 cover only about 5% of the full image).

Results obtained using KHB, supplemented with bovine serum albumin (BSA), are shown in the third row of images in Figure 5. The added BSA had the effect of reducing the mean size of agglomerates by a factor of 2.2 (similar to the results shown in Figure 3A). One consequence was a reduced speed of settling, the other a distinct change in the structure of particle pile-up at the bottom. Absolute data on settling velocities could not be derived, one reason being the limited resolution in optical imaging.

**Settling of Filtered Nanoaggregates.** In order to exclude the possibility that agglomerate formation at the bottom of the wells involved nonfractured large aggregates, a settling experiment was performed with a medium that had been filtered so that only nanoaggregates with sizes of less than 220 nm were left in the suspension. The agglomerates formed under these conditions grew to sizes between 2 and 10 $\mu$m (see Figure 6). A rough estimate shows that between 50 and 70% of the whole deposit is contained in ellipsoid-like agglomerates. Note that, within experimental uncertainty, the thickness (or volume) of the settled matter, roughly represented by the number of large aggregates, is proportional to the height of the medium, again in agreement with eq 2.

**Brownian-like Motion, the Key to Lateral Nanoaggregate Transport.** Details on Brownian-like motion are presented in Figure 7 for a sonicated powder of carbon single-wall nanotubes (SWNTs) in RPMI 1640 medium, supplemented with 10% fetal calf serum (FCS). The images represent the beginning (A) and end (B) of a movie (duration 2 min) recorded 18 h after deposition of the sonicated sample in the well (see Supporting Information). The three objects at which arrows are pointing have migrated, on average, a surprisingly large distance of about 10 $\mu$m within 2 min. Significant rotation of the large aggregates is also evident.

For the purpose of documenting that settling and Brownian-like motion occur quite generally with suspended nano- and microsized particles, two additional movies were made at much shorter times, $\Delta t$, after sample preparation, one for sonicated Printex 90 ($\Delta t$ = 1 h), the other for sonicated $TiO_2$(200), $\Delta t$ = 1.5 h (see Supporting Information). These movies also show particles traveling through the medium to the bottom.

**Effects of Illumination.** In course of this study, effects of sample illumination were observed repeatedly, but with distinctly different magnitudes for different combinations of nanopowder and liquid medium. The effect was first observed in studies that aimed at quantifying the speed of settling of $TiO_2$(80) in water by measuring time-dependent changes in absorbance in the central section of the analyzed medium. With increasing time of storage of the sample after sonication, a gradually increasing volume in the top part of the suspension (height typically 18 mm) turned transparent, quite well separated from the milky section

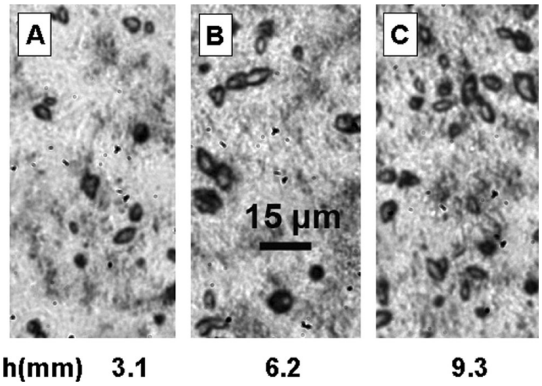


**Figure 6. Structure of deposits grown after $TiO_2$(80) nanoaggregates had completely settled at the bottom of cell culture wells filled with media of different heights *h*. The nanopowder was sonicated in KHB containing 7 mg/mL of BSA. Following sonication, the suspension was passed through a filter with a pore size of 220 $\mu$m. The filtered nanoaggregates had a mean size of 196 nm. At the quoted heights, the mass concentration of 55 $\mu$g/mL (calibrated by absorbance measurements) converts to total mean areal densities of (A) 17.5, (B) 35, and (C) 51.5 $\mu$g/cm$^2$ (corresponding compacted thicknesses 44, 88, and 132 nm, respectively).**

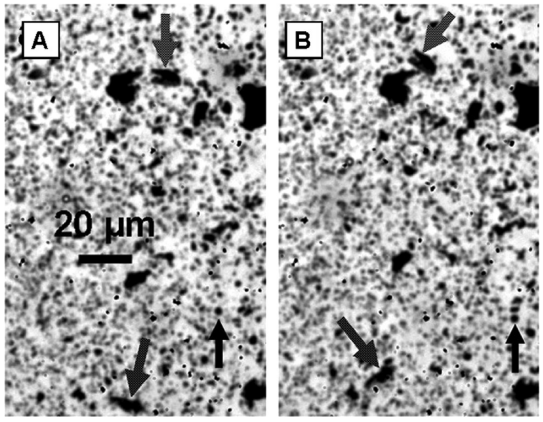


**Figure 7. Aggregates of carbon SWNTs settled at the bottom of a cell culture well, 18 h after sonication in RPMI 1640 medium. The initial mass concentration was 16 $\mu$g/mL, *h* = 6.2 mm. Presumably as an effect of illumination during imaging, a sizable fraction of the settled matter was relocated to a central area with a diameter of about 0.6 mm. Image B was taken 2 min after A.**

below. If the probing rectangular beam (*ca.* 2 × 10 mm) of monochromatic light (wavelength 380 nm) intersected the transition region between the two sections for more than about 20 s, deep troughs of transparent medium were generated in the milky section, thus strongly disturbing a correct measurement of the absorbance. Indications of this effect were also seen in DLS measurements. Apparently, the transition region between the transparent and the milky sections is highly unstable so that only a minor stimulation, presumable in the form of heat deposited by the incident light, suffices to cause very rapid and efficient diffusional transport of nanoaggregates.

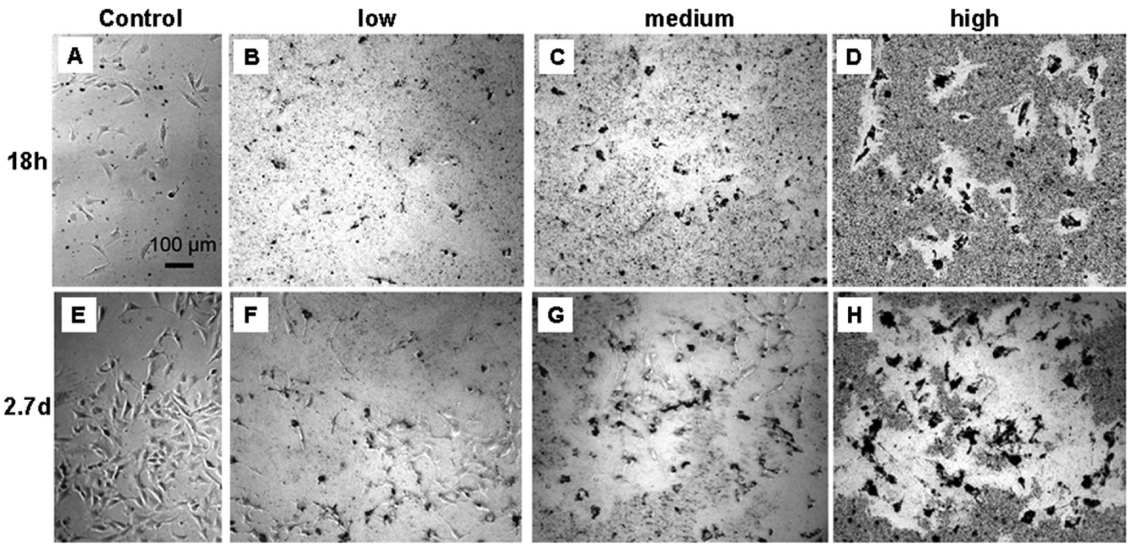


**Figure 8. Images illustrating the status of interaction of $Fe_2O_3$ particles with epithelial-like LA-4 cells of mice at two times of exposure in HAM's F12K medium. (A,E) Control sample, (B−D, F−H) exposed cells. The mass concentrations, the height of the media, and the calculated maximum thicknesses of settled matter were 33 $\mu$g/mL, 2.9 mm, and 18 nm in panels B and F ("low"), 33 $\mu$g/mL, 8.7 mm, and 55 nm in C and G ("medium"), and 96 $\mu$g/mL, 8.7 mm, and 160 nm in D and H ("high"). The cells were grown by T. Wachtmeister.**

Other effects of illumination were observed in the course of detailed studies on settling and Brownian-like motion of particles using optical microscopes. These investigations often required exposure of the samples to light for an extended period of time. The most obvious effect of this exposure was a change in the direction and the speed of particles on their way from the medium to the bottom, monitored by moving the plane of focus from the bottom into the medium (see movies 2 and 3). Occasionally, the effect of illumination was more pronounced, if not dramatic. Repeated redistribution of settled matter was observed, most strongly with samples containing carbon single-wall nanotubes (SWNTs). In another case, during an extended observation of SWNTs in water (+BSA at 0.9 mg/mL), essentially all of the settled matter suddenly moved out of focus. It turned out that it had been relocated, in some kind of concerted action, to one side of the well (see Figure 7). A similar effect was observed with a sample containing sonicated $TiO_2$ with primary particle sizes of about 200 nm. The phenomenon was not yet explored in detail.

**Nanoaggregate−Cell Interaction.** In view of the evidence presented above on settling and Brownian-like motion of particles in liquid media, it appeared desirable to take at least an exploratory look at the response of cells to the large amount of nanoaggregate matter available at the well bottom. Epithelial-like LA-4 cells of mice were exposed to $Fe_2O_3$ particles in HAM's F12K medium using 12-well plates. Exposure was deliberately started at a point of proliferation at which the coverage of the bottom was well below confluency (coverage *ca.* 15 ± 5%). The top-row images in Figure 8 depict the situation observed after 18 h of exposure. The columns labeled low, medium, and high relate to three different maximum areal densities of the nanoaggregate matter. It is evident at first sight that the presence of cells at the well bottom had a dramatic effect on the lateral distribution of settled matter. With increasing availability of particles, the cells had turned increasingly black, indicating that they had taken up or were covered with $Fe_2O_3$ matter (or both). Large areas surrounding the cells are seen to be devoid of particles. Both effects were more pronounced the larger the nominal coverage (or uptake). Other studies revealed similar features (LA-4 cells exposed to $TiO_2$(80), in collaboration with D. Adigüzel).

By way of moving the focal plane of the microscope through the region above the well bottom, the settled particles were found to execute Brownian-like motion preferentially within a roughly 5 $\mu$m thick layer above the well bottom. Assuming a medium with a height of typically 5 mm, this means that, under conditions of complete settling, the cells will be exposed to particles at a concentration exceeding the concentration in the as-prepared medium by a factor of 1000. Furthermore, as a result of lateral Brownian-like motion, the actual areal density of particles arriving at or attaching to cells is much higher than the mean coverage established at the well bottom where no cells are residing. The dose enhancement resulting from this effect will depend on the time of exposure. Analysis of the results of Figure 8H suggests that, with more or less isolated cells and after sufficiently long times of exposure (1−2 days), the amount of matter internalized in or accumulated on cells was at least an order of magnitude higher than the mean areal density of settled matter.

No attempt has yet been made to determine the fraction of dead cells in a quantitative manner. This

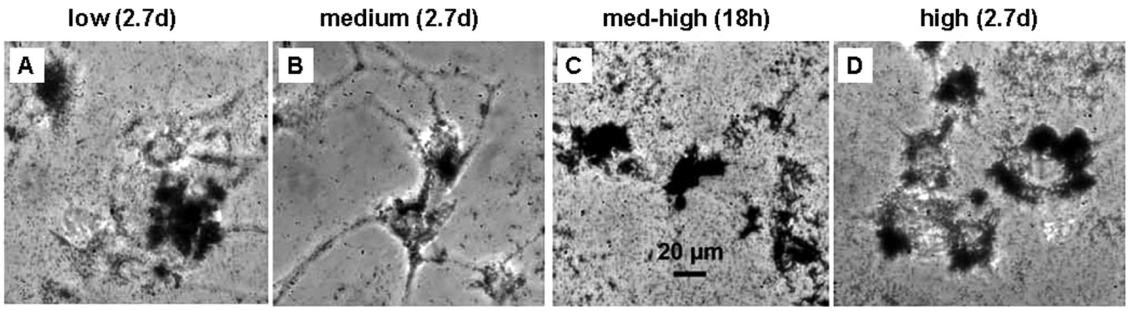


**Figure 9. Detailed view of the vital state of epithelial-like LA-4 cells after exposure to $Fe_2O_3$ NPs. The mass concentrations, the height of the media, and the calculated mean thicknesses of completely settled matter were (A) 33 $\mu$g/mL, 5.8 mm, and 36 nm, (B) 96 $\mu$g/mL, 2.9 mm, and 53 nm, (C) 96 $\mu$g/mL, 5.8 mm, and 107 nm, and (D) 96 $\mu$g/mL, 8.7 mm, and 160 nm.**

would make sense only if the vitality of each individual cell would be determined as a function of time and coverage. As Figure 9 shows, most of the heavily exposed cells are dead, in particular, those shown in panels C and D. This interpretation is supported by the fact that, in contrast to the control samples (Figure 8A,E), the density of cells did not increase with increasing time, notably for medium and high coverage (at low coverage the available images were not fully conclusive). Given the fact that the dead cells in Figure 8A,C,D are heavily loaded with particulate matter, there can be little doubt that they died because their vital functions were obstructed, largely or fully. At moderate load, however, cells may retain their vitality, as illustrated by the example shown in Figure 8B. In this case, nanotoxicity effects are not (yet) evident, even though, with about 200 to 300 $\mu m^2$ of the cell covered, some 5000 to 10 000 particles were available for interaction with the cell.

## DISCUSSION

Prior to discussing of the results, it worth noting that the aspects of nanotoxicity discussed here involve the idea that the mere physical presence of nanostructured matter in and on cells may cause adverse effects. More correctly, one should refer to this aspect as "physical nanotoxicity". It is well-known that the surface-to-volume or the surface-to-mass ratio increases with decreasing size of particles so that, dependent on the chemical properties of the solvent, the rate of dissolution of NPs (per unit mass, not per particle!)[27] may be high. If the dissolved material is toxic, as known for some ions of transition metals,[28,29] any associated adverse effects should be termed "chemical nanotoxicity". The resulting phenomena may be explored in analogy to the toxicological assessment of hazardous chemical substances. A much more difficult situation will be encountered if NPs are dissolved only by the time they have already been taken up by a cell.[29]

The results presented in Figure 8 validate the novel concept of cell exposure according to Figure 1B. Previous attempts to rationalize the results of *in vitro* cytotoxicity studies on the basis of the picture sketched in Figure 1A did not consider rapid settling of NPs. In terms of novel findings, the first important message is that the results of *in vitro* nanotoxicity studies are impossible to interpret unless the height of the cell culture medium is quoted in addition to other measures of dose such as the mass concentration, the mean particle size, and the time of exposure.

The second important message is that settled NPs perform intense Brownian-like motion, a finding that may serve to explain the results of Figure 8. Once the particles have arrived at the bottom of the well, they will travel, laterally and statistically, over distances on the order of tens or even hundreds of micrometers during the exposure period (owing to the fact that cells in incubators are kept at 37 °C, the mobility of particles in the experiment of Figure 8 was presumably larger than at room temperature to which the results of Figures 4–7 relate). Whenever the migrating NPs or NP aggregates encounter cells, the probability of uptake or adherence appears to be high. Particles taken up by cells or adhering to them are removed from the mobile fraction in the liquid medium. Hence the mean concentration near the cells will decrease significantly, so that this region looks empty. The concentration actually established will reflect the competition between the loss of particles to the cells and the influx from the high-concentration region.

The third important message concerns dose assessment in nanotoxicity studies. Given the fact that the arrival rate of particles at cells is generally unknown, a meaningful dose of exposure can only be defined if the amount of matter attached to or internalized by cells is measured. To add to the complications, the number of particles a cell will have access to depends on the spacing between neighboring cells; that is, the dose per cell will be much larger with isolated cells than with a confluent layer. Note that these arguments also hold if we assume that the empty regions around cells in Figure 8 are partly or fully due to motion of cells during the time of exposure.

An important question is whether delivery of particles to cells occurs only as long as the cells are alive. According to Figure 8, the size of the "emptied" areas increased after 18 h of exposure, even though many of the cells were already heavily loaded with matter at that time. This could mean that either the particles adhere not only to alive but also to dead cells or that even with a heavy

particle load the cells stay alive for a certain period of time, to the end that they die, in the experiment of Figure 8, at some point between 18 h and 2.7 days.

One of the aspects that could not be clarified in this work is the distinction between external and internal loading of cells with NP matter. Previous studies have concentrated on the analysis of NP uptake by cells. For that purpose, the cells were washed prior to further treatment. Element-specific analysis was carried out by inductively coupled plasma mass spectrometry (ICP-MS)[19,22] or atomic emission spectrometry (ICP-AES).[30] Careful cell washing, however, destroys the information on NP coverage of cells. Without documenting the coverage after exposure, one has no measure of dose for the individual cell studied; that is, one cannot correlate the number of possibly internalized particles with the amount of matter that was adhering to the cells before. Given the fact that NP uptake was found to saturate on time scales between 5 min[31] and 6 h,[30] it could well be that NP−cell interaction during a 24 h period of exposure will take place in two steps, first efficient internalization up to saturation followed by deposition of settled matter on the cells. Distinction between these two fractions appears to be highly relevant for an understanding of cytotoxicity effects. It will also be necessary to address the question whether saturation is a matter of time or the amount of internalized matter, or both. Whereas the speed of NP uptake (by number) was found to be size-dependent,[30] cells do not seem to have problems with the internalization of large agglomerates.[19] Even particles with sizes of several micrometers were found to be internalized by A549 human lung epithelial cells.[32] Note that uptake of NPs by cells does not necessarily cause acute cytotoxicity, as shown for gold particles.[33]

One conceivable avenue of future research is online microscopic imaging of the interaction of settled particles with individual cells. Such investigations will require highly dedicated instrumentation, like incubators with integrated inverted microscopes. The ultimate problem of such studies may be the Brownian-like motion of particles, which has the effect of leaving the control of the location of particle adherence to the cell, not to the experimenter. Various other suggestions for future work have been discussed elsewhere.[18]

## CONCLUSIONS

The results presented above imply that a large fraction of previous studies aimed at exploring the health hazard associated with exposure to NPs may not have been as conclusive as desired. In many cases, the observed effects were presumably not due to the (unknown) toxic potential of the particles but rather a consequence of mechanically obstructing the vital functions of cells by way of overloading them internally or externally with insoluble matter. It may be worth the effort to re-evaluate previous studies with the aim of identifying those cases where the observed effects were actually due to cell overload. The situation is reminiscent of the early overload studies with animals.[34,35] In both cases, the most adequate measure of exposure appears to be the volume of matter available to or deposited on the cells. In cell culture studies, the internalized and the deposited NPs will initiate a whole spectrum of time-dependent responses, the end point being cell death. The measured "mean" signal will be a very ill defined average over the responses sent out at different times of exposure, and from cells with a wide range of loading with nanostructured matter. Hence, there is a need for studies with highly efficient, short-term delivery of NP matter to cells, followed by extended periods of cell culture in clean media.

These ideas may be carried even further. As shown in another very closely related study,[18] adverse effects due to exposure of submersed cells to nanostructured matter are only observed if the dispersed material is transported fairly rapidly to the cells, by gravitational settling and/or by diffusion.[19] Hence, there is no reason to strive for a uniformly mixed, "stable" dispersion of NPs in the medium. The apparent need for a stable dispersion was nurtured, knowingly or unknowingly, by analogy arguments in memory of procedures used to assess the risk due to exposure to hazardous chemical substances. Stable dispersions, if they can really be produced, will merely have the effect of slowing down the rate of NP−cell contact. It may well be of interest to study the fate of cells under conditions of "slow" exposure, but on the standard time scale of 24 h, the result may only be: no effect. To get close to the situation sketched in Figure 1A, researchers should grow the cells at the walls of the well so that the cells will not be exposed to settled material (but NP transport to cells by diffusion would still occur). However, what we really wish to know is the following: How do cells respond if a certain number of NPs arrive at their outer surface? It is unlikely that the response will depend on the history of NP travel to the cells. The parameters that we need to get proper control of are the amount of NP matter delivered to the cells, the frequency of exposure (once or repeatedly), and the time after exposure. In other words, it is about time for a paradigm shift in the design of nanotoxicity studies.

## METHODS

**Particles.** The following nanopowders were used (the numbers in parentheses denote the nominal primary particle size in nanometers according to the manufacturer): $TiO_2$(20), $TiO_2$(250), Printex 90 (all by Degussa), Aerosil (Degussa Evonik), carbon single-wall nanotubes, SWNTs (Sigma-Aldrich), $TiO_2$(80) (TAL), $SiO_2$(80), $Fe_2O_3$(60), $Fe_3O_4$(25), Co(30), $CeO_2$(100)

(Nanoamor). The powders were kindly made available by M. Maier, Institute of Toxicology, and by A. Gatti, Modena, Italy.

**Particle Treatment and Size Analysis.** The model UW 2070 probe-type sonicator (Bandelin) served to fracture aggregates suspended in different liquids. Carefully weighed quantities of nanostructured matter were deposited at the conical bottom end of a test glass with an inner diameter of 14 mm. Five to 7 mL of solvent was added gently. Sonication was carried out with the tip of the probe inserted by $6 \pm 1$ mm. Size spectra of particles were determined by dynamic light scattering (DLS) using the high-performance particle sizer (HPPS, Malvern), operating at a wavelength of 632.8 nm and a scattering angle of 173°. The liquid samples were contained in cuvettes with an inner cross section of $4 \times 10$ mm$^2$; the height of the liquid was typically 18 mm. Usually, three DLS spectra were taken with an integration time of 30 s each. The size and morphology of individual particles and aggregates were explored by scanning electron microscopy (SEM), using a model JSM-6300F SEM (JEOL) equipped with a field emission electron gun.

**Quantification of Particle Settling.** One approach to determining the speed of sedimentation was to measure the absorbance of light as a function of time using samples in cuvettes used for DLS. The employed spectrophotometer (Uvikon 941 plus, Kontron Instruments) was set for analysis at a wavelength of 380 nm. The measured signal represents the absorbance averaged over a 10 mm wide vertical section of the liquid, defined by slits in the spectrophotometer. The slits are roughly centered at half height of the analyzed liquids (one sample and one reference without particles).

More direct information on gravitational settling was obtained by monitoring the arrival rate of sonicated matter at the bottom of wells. Three different inverted microscopes served the purpose, Axiovert 2000, Axiovert 200 M, and Axio Observer Z1, all by Zeiss. The instruments were operated at magnifications between 10× and 63×. The Axio Observer Z1 was also used to produce movies of particle motion during and after settling.

**Cell Cultures.** Adherent epithelial-like LA-4 cell were kindly provided by M. Semmler-Behnke. The cell line was isolated from urethane-induced lung adenoma of an A/He strain mouse (28 weeks of age). The cells, previously used successfully in exposure studies (D. Adigüzel, personal communication), were cultured in a model 3111 S/N incubator (Forma Scientific) under standard conditions (37 °C, 5% $CO_2$).

*Acknowledgment.* I thank several colleagues for supporting this study in many different ways. A. Stampfl, M. Maier, and J. Lichtmannegger provided access to and assistance with techniques for particle characterization, T. Wachtmeister prepared cell cultures, and H. Wehnes produced high-quality electron micrographs.

*Supporting Information Available:* Additional details in movies. This material is available free of charge *via* the Internet at http://pubs.acs.org.

## REFERENCES AND NOTES

1. Gwinn, M. R; Vallyathan, V. Nanoparticles: Health Effects—Pros and Cons. *Environ. Health Perspect.* **2006,** *114*, 1818–1825.
2. Tsuji., J. S.; Maynard, A. D.; Howard, P. C.; James, J. T.; Lam, C.-W.; Warheit, D. B.; Santamaria, A. B. Research Strategies for Safety Evaluation of Nanomaterials, Part IV: Risk Assessment of Nanoparticles. *Toxicol. Sci.* **2006,** *89*, 42–50.
3. Dunphy Guzmán, K. A.; Taylor, M. R.; Banfield, J. F. Environmental Risks of Nanotechnology: National Nanotechnology Initiative Funding 2000—2994. *Environ. Sci. Technol.* **2006,** *40*, 1401–1407.
4. Dobrovolskaia, M. A.; McNeill, S. E. Immunological Properties of Engineered Nanomaterials. *Nat. Nanotechnol.* **2007,** *2*, 469–478.
5. Oberdörster, G.; Stone, V.; Donaldson, K. Toxicology of Nanoparticles: A Historical Perspective. *Nanotoxicology* **2007,** *1*, 2–25.
6. Dobson, J. Toxicological Aspects and Applications of Nanoparticles in Paediatric Respiratory Disease. *Paed. Respir. Rev.* **2007,** *6*, 62–66.
7. Buzea, C.; Pacheco, I. I.; Robbie, K. Nanomaterials and Nanoparticles: Sources and Toxicity. *Biointerphases* **2007,** *2*, MR17–71.
8. Lewinski, N.; Drezek, R.; Colvin, V. Cytotoxicity of Nanoparticles. *Small* **2008,** *4*, 26–49.
9. Brayner, R. The Toxicological Impact of Nanoparticles. *Nanotoday* **2008,** *3*, 48–55.
10. Kroll, A; Pillukat, M. H.; Hahn, D.; Schnekenburger, J. Current *In Vitro* Methods in Nanoparticle Risk Assessment: Limitations and Challenges. *Eur. J. Pharm. Biopharm.* **2009,** *72*, 370–377.
11. Tervonen, T.; Linkov, I.; Figuera, J. R.; Steevens, J.; Chappell, M.; Merad, M. Risk-Based Classification System of Nanomaterials. *J. Nanopart. Res.* **2009,** *11*, 757–766.
12. Auffan, M.; Rose, J.; Bottero, J.-Y.; Lowry, G. V.; Jolivet, J.-P.; Wiesner, M. R. Towards a Definition of Inorganic Nanoparticles from an Environmental, Health and Safety Perspective. *Nat. Nanotechnol.* **2009,** *4*, 634–641.
13. Fadeel, B.; Garcia-Bennett, A. E. Better Safe than Sorry: Understanding the Toxicological Properties of Inorganic Nanoparticles Manufactured for Biomedical Applications. *Adv. Drug Delivery Rev.* **2010,** *62*, 362–374.
14. Fubini, B.; Ghiazza, M.; Fenoglio, I. Physico-Chemical Features of Engineered Nanoparticles Relevant to Their Toxicity. *Nanotoxicology* **2010,** *4*, 347–363.
15. Gil, P. R.; Oberdörster, G.; Elder, A.; Puntes, V.; Parak, W. J. Correlating Physico-Chemical with Toxicological Properties of Nanoparticles: The Present and the Future. *ACS Nano* **2010,** *4*, 5527–5531.
16. Stark, J. W. Nanoparticles in Biological Systems. *Angew. Chem., Int. Ed.* **2011,** *50*, 1242–1258.
17. Limbach, L. K.; Grass, R. N.; Stark, W. J. Physico-Chemical Differences between Particle- and Molecule Derived Toxicity. *Chimia* **2009,** *63*, 38–43.
18. Wittmaack, K. Novel Dose Metric for Apparent Cytotoxicity Effects Generated by *In Vitro* Cell Exposure to Silica Nanoparticles. *Chem. Res. Toxicol.* **2011,** *24*, 150–158.
19. Limbach, L. K.; Li, Y.; Grass, R. N.; Brunner, T. J.; Hintermann, M. A.; Muller, M.; Gunther, D.; Stark, W. J. Oxide Nanoparticle Uptake in Human Lung Fibroblasts: Effects of Particle Size, Agglomeration, and Diffusion at Low Concentrations. *Environ. Sci. Technol.* **2005,** *39*, 9370–9376.
20. Bihari, P.; Vippola, M.; Schultes, S.; Praetner, M.; Khandoga, A. G.; Reichel, C. A.; Coester, C.; Tuomi, T.; Rehberg, M.; Krombach, F. Optimized Dispersion of Nanoparticles for Biological *In Vitro* and *In Vivo* Studies. *Particle Fibre Toxicol.* **2008,** *5*, 14.
21. Volckens, J.; Dailey, L.; Walters, G.; Devlin, R. B. Direct Particle-to-Cell Deposition of Coarse Ambient Particulate Matter Increases the Production of Inflammatory Mediators from Cultured Human Airway Epithelial Cells. *Environ. Sci. Technol.* **2009,** *43*, 4595–4599.
22. Lison, D.; Thomassen, L. C. J.; Rabolli, V.; Gonzalez, L.; Napierska, D.; Seo, J. W.; Kirsch-Volders, M.; Hoet, P.; Kirschhock, C. E. A.; Martens, J. A. Nominal and Effective Dosimetry of Silica Nanoparticles in Cytotoxicty Assays. *Toxicol. Sci.* **2008,** *104*, 155–162.
23. Ju-Nam, Y.; Lead, J. R. Manufactured Nanoparticles: An Overview on Their Chemistry, Interactions and Potential Environmental Implications. *Sci. Total Environ.* **2008,** *400*, 96–414.
24. Murdock, R. C.; Braydich-Stolle, L.; Schrand, A. M.; Schlager, J. J.; Hussain, S. M. Characterization of Nanomaterial Dispersion in Solution Prior to *In Vitro* Exposure Using Dynamic Light Scattering Technique. *Toxicol. Sci.* **2008,** *101*, 239–253.
25. Zhang, Y.; Chen, Y.; Westerhoff, P.; Hristovski, K.; Crittenden, J. C. Stability of Commercial Oxide Nanoparticles in Water. *Water Res.* **2008,** *42*, 2204–2212.
26. Wittmaack, K. Comprehensive Characterization of Manufactured Nanoscaled Powders Following Soft Dispersion. European Aerosol Conference EAC 2009, Book of Abstracts, 2009, Paper #T190A07.
27. Wittmaack, K. Dose and Response Metrics in Nanotoxicology: Wittmaack Responds to Oberdoerster *et al.* and Stoeger *et al. Environ. Health Perspect.* **2007,** *115*, A291–292.

28. Brunner, T. J.; Wick, P.; Manser, P.; Spohn, P.; Grass, R. N.; Limbach, L. K.; Bruinink, A.; Stark, W. J. *In Vitro* Cytotoxicity of Oxide Nanoparticles: Comparison to Asbestos, Silica, and the Effect of Particle Solubility. *Environ. Sci. Technol.* **2006,** *40*, 4374–4381.
29. Limbach, L. K.; Wick, P.; Manser, P.; Grass, R. N.; Bruinink, A.; Stark, W. J. Exposure of Engineered Nanoparticles to Human Lung Epithelial Cells: Influence of Chemical Composition and Catalytic Activity on Oxidative Stress. *Environ. Sci. Technol.* **2007,** *41*, 4158–4163.
30. Chithrani, B. D.; Ghanzani, A. A.; Chan, W. C. W. Determining the Size and Shape Dependence of Gold Nanoparticle Uptake into Mammalian Cells. *Nano Lett.* **2006,** *6*, 662–668.
31. Moss, O. R.; Wong, V. A. When Nanoparticles Get in the Way: Impact of Projected Area on *In Vivo* and *In Vitro* Macrophage Function. *Inhal. Toxicol.* **2006,** *18*, 711–716.
32. Fanizza, C.; Ursini, C. L.; Paba, E.; Ciervo, A.; Di Francesco, A.; Maiello, R.; De Simone, P.; Cavallo, D. Cytotoxicity and DNA-Damage in Human Lung Epithelial Cells Exposed to Respirable α-Quartz. *Toxicol. In Vitro* **2007,** *21*, 586–594.
33. Connor, E. E.; Mwamuka, J.; Gole, A.; Murphy, C. J.; Wyatt, M. D. Gold Nanoparticles Are Taken up by Human Cells but Do Not Cause Acute Cytotoxicity. *Small* **2005,** *1*, 325–327.
34. Morrow, P. E. Possible Mechanisms To Explain Dust Overloading of the Lung. *Fundam. Appl. Toxicol.* **1988,** *10*, 369–384.
35. Mauderly, J. L. Lung Overload: The Dilemma and Opportunities for Resolution. *Inhal. Toxicol.* **1996,** *8* (Suppl.), 1–29.